INFLUENCE OF STRUCTURE AND HYDROPHOBIC PROPERTIES ON THE CHARACTERISTICS OF CARBON–AIR ELECTRODES*

G. V. SHTEINBERG, A. V. DRIBINSKY and I. A. KUKUSHKINA

Institute of Electrochemistry of the USSR Academy of Sciences, Leninsky Prospekt, 31, 117071 Moscow, V-71 (USSR)

M. MUSILOVÁ and J. MRHA

J. Heyrovsky Institute of Physical Chemistry and Electrochemistry, Czechoslovac Academy of Sciences, Prague 10 (Czechoslovakia)

(Received June 26, 1981)

Summary

The electrochemical parameters of carbon–oxygen gas-diffusion electrodes can be controlled over a wide range by varying the structure of the active carbon catalyst and the ratio of lyophilic and lyophobic pores in the catalyst particles. Two typical representatives of active carbon catalysts with significantly different hydrophobic properties have been investigated by mercury–alkali intrusion porosimetry and tested both in model floating electrodes and as the hydrophilic component of the active layer of two-layer, gas-diffusion working electrodes. The optimal electrolyte content in the active layer ensuring the maximum electrical characteristics of working electrodes has been found to depend on the structure and hydrophobic properties of the carbon catalyst. The gas pores in the carbon catalyst have been shown to play an essential role in the oxygen mass transfer process in the active layer.

Introduction

Porous carbon base gas-diffusion electrodes for the reduction of oxygen in alkaline solutions have been attracting the attention of investigators for many years. At present there are two kinds of such electrodes, depending on their application: electrodes for fuel cells and electrodes for metal–air systems. Application in fuel cells is connected with operation at high loads up to some hundreds of mA/cm^2. Only promoted carbon electrodes working at elevated temperatures (~ 70 °C) and containing silver, organic N_4-chelates, spinel oxides or platinum metals can satisfy these requirements. The problem

*Paper presented at the 2nd Czechoslovak International Conference on Electrochemical Power Sources, Žilina, Czechoslovakia, June 22 - 26, 1981.

0378-7753/82/0000-0000/$02.75

of electrocatalysts in air electrodes for alkaline metal–air systems can be solved with the use of a pure, active carbon catalyst, since the current densities in their case are almost an order less than in fuel cells. This considerably reduces the cost of air electrodes. In cases where it is necessary to work at higher loads, impregnation of carbon cathodes with very small amounts of silver or platinum provides a solution to the problem.

For these reasons a thorough investigation of different active carbons is of interest both in respect of their catalytic activity and their structure and lyophobic properties. The next problem is to find the optimal means of introducing active carbon particles into the porous structures of the active layer, *i.e.*, the choice of the technological parameters for the manufacture of electrodes with the required characteristics, including working current density, service life, conditions and regime of operation, etc. Here the dominant role is played by the ratio of liquid and gas (*i.e.*, lyophilic and lyophobic) pores in the active layer, which determines the mass transfer conditions.

At present two types of electrodes based on active carbon have been developed. In the first type the active layer consists of a mixture of active carbon and polytetrafluoroethylene (PTFE) particles, and the watertight gas-supplying layer consists only of PTFE particles [1 - 4]. The active layer of the second type of electrode is a mechanical mixture of active carbon catalyst and a hydrophobic component prepared by PTFE deposition on different conducting materials, *e.g.*, on carbon black. The gas-supplying layer of the second type of carbon electrode is formed from the same hydrophobic component [5 - 7]. An advantage of this material is that along with high hydrophobic properties, it also has adequate conductivity. This allows the ratio of hydrophobic and hydrophilic components of the active layer to be varied within wide limits.

The second type of electrode was used in our measurements for studying the influence of the structure and lyophobic properties on the electrical characteristics of both oxygen and air cathodes.

Experimental

For the investigation of the porous structure and hydrophilic–hydrophobic properties of the carbon electrode and its individual components we used mercury–alkali intrusion porosimetry [8 - 10].

The technique is based on comparison of the mercury and alkali intrusion curves. The surface tension of mercury is constant (σ_{Hg} = 480 dyne/cm) and the contact angle, θ_{Hg}, usually depends slightly on the nature and dispersion of the solid (θ_{Hg} = 130 - 150°); the mercury intrusion curves allow quantitative determination of the parameters ($\partial v/\partial r$) of the porous structure of any porous body by the equation:

$$r = -\frac{2\sigma \cos\theta}{P} \tag{1}$$

where r is the pore radius and P the applied pressure.

If mercury is replaced by an alkaline electrolyte, then even before application of an excess pressure, the lyophilic (relative to the given electrolyte) pores are filled with liquid and the intrusion curve describes only the filling of lyophobic pores*. With the same order of pore filling with mercury and electrolyte, the contact angle of lyophobic pores with electrolyte can be determined by the equation

$$\Delta \lg P = \lg \frac{\sigma_{Hg} \cdot \cos \theta_{Hg}}{\sigma_{KOH} \cdot \cos \theta_{KOH}}, \quad (2)$$

where $\Delta \lg P$ is the distance between the mercury and the electrolyte intrusion curves. Equations (1) and (2) permit calculation of the dependence of the pore volume and contact angle on the radius, *i.e.*, a complete description of the capillary properties of lyophobic pores and estimation of the volume of lyophilic pores. It is necessary to take into account the fact that in the presence of large pores the absence of an exact knowledge of where the mercury and electrolyte intrusion curves start can have a considerable influence on the results. For this reason, when processing the experimental data, in plotting the curve we did not use the volume of liquid, V, impressed into the pores at a given pressure P, but the volume of the void pores $\bar{V} = V_0 - V$, where V_0 is the total volume of pores in the specimen.

As a model electrode we used a floating gas-diffusion electrode in the form of a very thin carbon layer (no more than 1 mg/cm^2) on a porous hydrophobic conducting substrate. Carbon was applied to the porous substrate without a binder and was not subjected to any heat treatment; it was retained on the hydrophobic surface by adhesion alone. The electrode was placed into an hermetic glass cell, so that the hydrophobic substrate was located in the gas phase and the catalyst was immersed in electrolyte. As shown in ref. 11, on such an electrode in 1N KOH in the range from steady-state to working potentials (polarization 0.15 - 0.20 V) in pure oxygen and air–oxygen, the electrode operates in the kinetic regime, *i.e.*, the carbon surface is equally accessible for the oxygen reduction reaction. This is evidenced by the first order reaction in oxygen, by the independence of the specific activity (mA/g) of the weighted amount of carbon, and by the high values of the activation energy [11].

The visible working surface of the model electrode used was 1 cm^2. The amount of carbon in contact with the electrolyte and substrate was calculated from comparison of the apparent double layer capacity of the electrode with the capacity of one gram of carbon powder [12]. These quantities were determined by recording the potentiodynamic charging curves (V = 0.2 - 2 mV/s) in helium [11].

---

*Since the wetting of carbon by water and concentrated alkaline solution can differ significantly [9], *e.g.*, in some cases hydrophilic pores are not wetted by alkali ($\theta_{H_2O} < 90°$, $\theta_{KOH} > 90°$), we shall further use the terms "lyophobic, lyophilic" to denote the wettability in 7N KOH.

The apparent double layer capacity of the substrate, as well as the oxygen reduction currents on it, were less than 10% of the corresponding values for the electrode with the carbon and for this reason they were not taken into account.

With the use of this model electrode the electrocatalytic activity of the two types of carbon, AG-3 (S_{BET} — 1200 m^2/g) and HS-4 (S_{BET} — 915 m^2/g), was compared in 1N and 7N KOH in pure oxygen and in air–oxygen. Some experiments were also carried out on Norit-NK carbon (S_{BET} — 635 m^2/g), widely used in electrodes of the second type [5 - 7]. The current density at E_r = 0.9 V and 0.83 V was taken as a measure of the electrode activity.

The working carbon electrodes with PTFE binder consisted of a semi-hydrophobic active layer composed of a mechanical mixture (30 mg/cm^2) of different active carbon catalysts (particle size < 60 μm) and the hydrophobic component (carbon black waterproofed with 35% PTFE), and a strongly hydrophobic, watertight, gas-supplying layer prepared from the hydrophobic component only (100 mg/cm^2).

AG-3 and HS-4 active carbons were used as catalysts. The hydrophobic component was prepared from acetylene black P-1042 (DDR) and a PTFE GP-I suspension. The composition of the active layer is denoted by two numbers, the first corresponding to the active carbon fraction, the second to that of the hydrophobic component (*e.g.*, the active layer of mix 3-2 corresponds to 18 mg/cm^2 of active carbon and to 12 mg/cm^2 of hydrophobic component).

Disc electrodes with 5 cm^2 electrolyte contact area and thickness 1.1 - 1.7 mm (depending on the active layer mix), prepared by hot pressing (350 °C, 20 MPa), were used in all measurements. A current collector (nickel plated steel grids) was pressed onto both sides of the electrode.

The steady-state current–voltage characteristics were measured using a conventional half-cell with a nickel plate counter electrode and a Hg/HgO reference electrode. Measurements were carried out in 7N KOH at normal temperature both for pure oxygen and air–oxygen (1 cm H_2O overpressure) after electrode operation in pure oxygen for 15 h at a current load of 100 mA/cm^2.

From the current–voltage curves both for pure oxygen and air–oxygen the $\Delta E(i)$ characteristics were calculated [12 - 15]. The $\Delta E(i)$ values correspond to the shift of the electrode potential, ΔE, when the gas supply is switched from pure oxygen to air–oxygen at a definite current load, i (no influence of the iR drop):

$$\Delta E(i) = E_{O_2}(i) - E_{air}(i).$$

The amount of electrolyte that soaked into the active layer was estimated from the weight increase of the electrode at the end of the electrochemical measurements.

All electrochemical data obtained from electrode measurements using two-layer electrodes are given as the following basic electrode parameters:

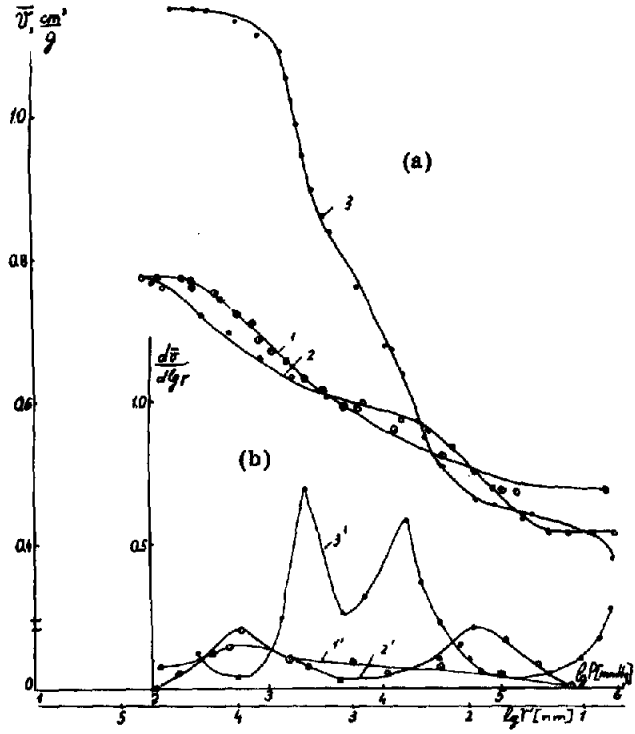

Fig. 1. Integral (a) and differential (b) mercury intrusion curves for active carbons: 1, granulated HS-4; 2, broken up HS-4; 3, granulated AG-3.

i_{100} — current density (mA/cm^2) with pure oxygen at potential $E = -100$ mV (*vs.* Hg/HgO); ΔE_{100} — shift of electrode potential when pure oxygen is replaced by air–oxygen at a current density of 100 mA/cm^2; G — amount of electrolyte (g of 7N KOH per 1 g of electrode active layer) after 7 days operation under current load and 2 h without load for equalising the catholyte and bulk electrolyte concentrations; G^* — amount of electrolyte in 1 g of active carbon, which is the only hydrophilic component of the active layer; i_{O_2}/i_{air} — ratio of current density for pure oxygen (i_{O_2}) and air (i_{air}) at the same electrode potential, E.

Results and discussion

1. Mercury intrusion porosimetry

1.1. Active carbon

In Fig. 1 integral (a) and differential (b) mercury intrusion curves are given for initial granules of HS-4 and AG-3 active carbons (curves 1, 3) and also for broken up granules of HS-4 (curve 2).

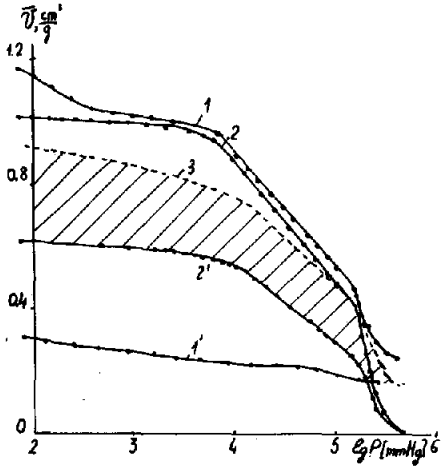

Fig. 2. Integral mercury intrusion curves for a two-layer electrode: 1, active layer (mix 2-3); 2, watertight gas-supplying layer; 1′ and 2′, partial mercury intrusion curves for HS-4 carbon (1′) and for the hydrophobic component of the active layer (2′); 3, the sum of the partial curves.

It is evident from curves 1 and 3 that the total volume of pores in HS-4 is ~0.8 cm^3/g and in AG-3 ~1.15 cm^3/g. The volume of pores with $r = 2 \times 10^4 - 2 \times 10^2$ nm, *i.e.*, the volume of macropores [14] is 0.3 cm^3/g and 0.8 cm^3/g, and the volume of small pores with a radius up to 10 nm is 0.45 cm^3/g and 0.38 cm^3/g, respectively. Thus, the volume of macropores in carbon HS-4 is nearly 2.5 times less than in AG-3, whereas the volume of small pores is approximately 20% higher. After breaking up HS-4 granules the shape of the intrusion curve and the total pore volume remain almost unchanged.

AG-3 and HS-4 active carbons also differ significantly in the pore-radii distribution. For granules of AG-3 two maxima are typical, at $r_1 = 2.8 \times 10^3$ and at $r_2 = 3 \times 10^2$ nm. The distribution curve for granules of HS-4 has no clear maximum (Fig. 1b).

1.2. Active and watertight gas-supply layers

The intrusion curves of the active layer (HS-4, mix 2-3) and the watertight layer are shown in Fig. 2. In the watertight layer there are practically no pores of radius exceeding 2500 nm. The maximum on the differential pore-radii distribution curve corresponds to pores with $r = 17$ nm. To estimate the contribution of the active layer components to the pore volume for different radii we calculated the partial intrusion curves corresponding to the content of HS-4 carbon (Curve 1′) and the hydrophobic component (Curve 2′) in one gram of the active layer. When comparing Curves 1′, 2′ and 1 one can clearly distinguish the mercury intrusion regions for HS-4 carbon and for the hydrophobic component. The hydrophobic component makes the main contribution to the total volume of the active layer pores, and HS-4 carbon to the

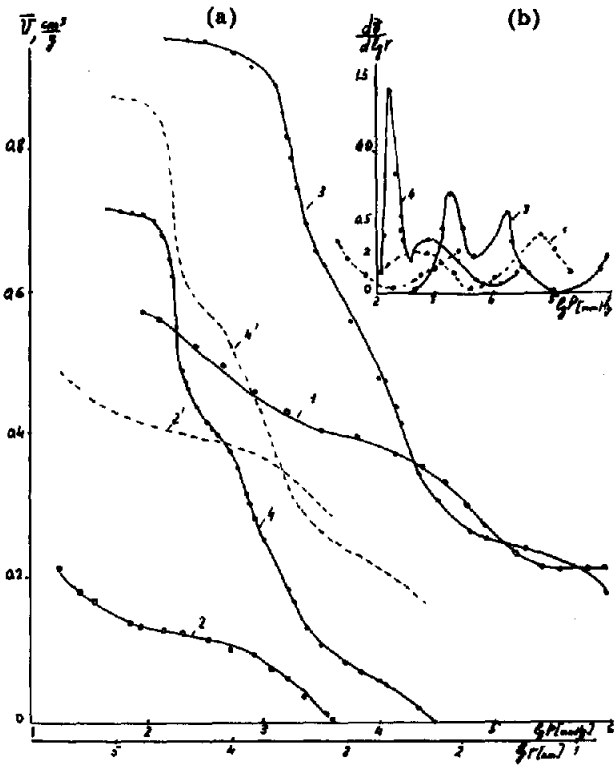

Fig. 3. Integral (a) and differential (b) mercury (1,3) and alkali (2,2', 4,4') intrusion curves for active carbons: 1,2, granulated HS-4; 3,4, granulated AG-3; 2' and 4' are curves 2 and 4 made coincident in their characteristic points with the mercury curves.

volume of pores with $r > 1000$ nm. It should be noted that the experimental mercury intrusion curve (Curve 1) lies higher than the sum of the partial curves (the hatched area corresponds to the pore volume in HS-4 carbon contained in one gram of the active layer). This indicates the appearance of additional volume (secondary structure pores) during the active layer formation.

2. Comparison between mercury and alkali intrusion curves

2.1. Active carbon

The alkali and mercury intrusion curves for granules of HS-4 and AG-3 active carbons are presented in Fig. 3. It is evident from comparison of Curves 2 and 4 that HS-4 contains a much smaller (approximately 4 times less) volume of lyophobic pores than does AG-3.

In order to estimate the contact angle, the alkali intrusion curves were displaced along the ordinate until the characteristic points on the mercury and alkali curves coincided [9]. Then the mercury and electrolyte curves for AG-3 (Curves 3 and 4') become almost parallel in a wide pressure range, which indicates that the contact angle with electrolyte is constant in a wide

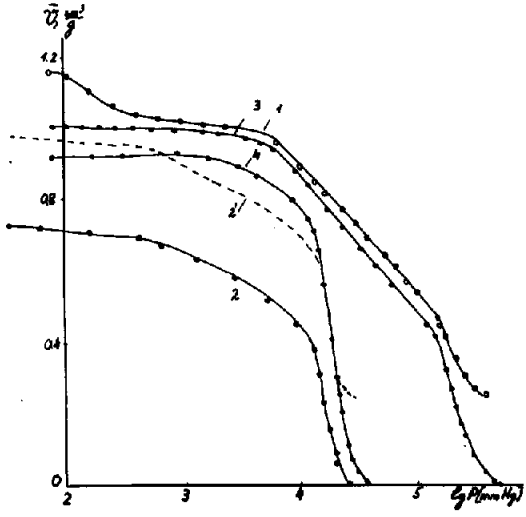

Fig. 4. Mercury (1,3) and alkali (2,2',4) intrusion curves for the active and the watertight layers of two-layer electrodes: 1,2, active layer (mix 2-3); 3,4, watertight layer; 2' is curve 2 made coincident with the mercury curve.

pore size range. Calculation by eqn. (2) gives a value of $\theta_{KOH} = 104°$ for AG-3 macropores. The electrolyte and mercury intrusion curves for HS-4 (Curves 1 and 2') are parallel in a narrow range of pore sizes ($r = 10^3 - 10^2$ nm), for which calculation gives $\theta_{KOH} = 103°$.

2.2. Active and watertight gas-supplying layers.

The mercury and alkali intrusion curves showing the distribution of lyophobic pores in an active layer 2-3 with HS-4 carbon, and in the watertight gas-supply layer, are presented in Fig. 4. As can be seen from the Figure, more than 90% of the pore volume in the gas-supply layer are lyophobic pores, their contact angle with alkali being equal to 113 - 115°. In the active layer of the above mentioned composition about 80% of the macropore volume are lyophobic also with respect to alkali. The lyophobic porosity of the active layer is determined by the fraction of the hydrophobic component in the mixture with active carbon; this is particularly clear from Fig. 5, where the alkali intrusion curves for individual components of the active layer and for their two mixtures (2-1, 2-3) are compared with the partial curves (the hatched area corresponds to the volume of lyophobic pores in the carbon contained in one gram of the active layer). It is also seen from Fig. 5, that the lyophobic porosity of the active layer is somewhat higher than the sum of the lyophobic porosities of the individual layer components (curves 3 and 5, 4 and 6); this can be explained by the formation of secondary structure pores. Comparison of the curves for the active layer (Figs. 2 and 5) leads to the conclusion that the secondary structure pores produced during the formation of the active layer are mainly lyophobic but start to be filled with

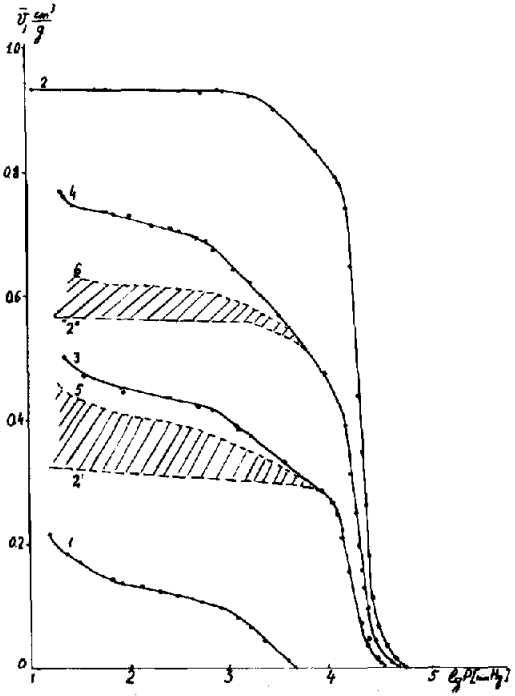

Fig. 5. Alkali intrusion curves for active layers and their individual components: 1, granulated HS-4; 2, watertight layer; 3, active layer (mix 2-1); 4, active layer (mix 2-3); 2',2'', partial curves for the hydrophobic component of layers 2-1 and 2-3, respectively; 5,6, the sum of the partial curves for layers 2-1 and 2-3, respectively.

electrolyte at low pressure. These pores, probably, correspond to the gaps between active carbon grains and waterproofed carbon black particles.

It should be emphasized that the curves were obtained on fresh active layer specimens after a short (2 h) contact with alkali electrolyte. In the working two-layer electrode which was used for the electrochemical measurements after a 15 h polarization with a 100 mA/cm^2 load, the lyophobic porosity should be less as a result of lyophilization of a part of the pores, including secondary structure pores.

3. Electrochemical measurements

3.1. Model electrode

The oxygen reduction polarization curves on a model electrode with three different carbon catalysts — HS-4, AG-3 and Norit-NK in 1N KOH — are shown in Fig. 6. For all types of carbon the curves have a constant Tafel slope in the range of almost three orders of current, which is equal to 45 mV for HS-4 carbon and 50 - 55 mV for AG-3 and Norit-NK carbons. The curves in air are parallel to similar curves in oxygen (Fig. 6, curves 2 and 4). The ratio of the currents is i_{O_2}/i_{air} = 4.8 - 5.0, *i.e.*, it corresponds to the first order reaction in oxygen (Table 1). Accordingly, $\Delta E(i)$ = 30 mV for HS-4

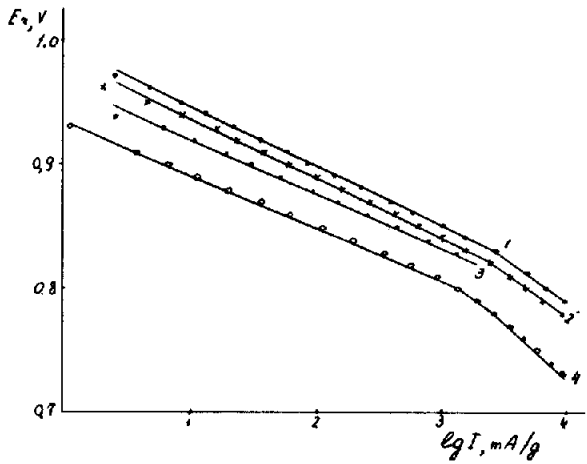

Fig. 6. Polarisation curves of oxygen reduction on different carbon catalysts in a model floating electrode: 1, active carbon AG-3; 2,4, active carbon HS-4; 3, active carbon Norit-NK; 1-3, oxygen; 4, air.

TABLE 1

Electrochemical characteristics in a model floating electrode

Type of carbon	Activity in O_2, mA/g at:			$\frac{i_{O_2}}{i_{air}}$ (at E_r = 0.9 V)		$\partial E/\partial \lg i$ (mV)	
	E_r = 0.9 V		E_r = 0.83 V				
	1N KOH	7N KOH	7N KOH	1N KOH	7N KOH	1N KOH	7N KOH
HS-4	30	190	5230	4.8	4.4	45	45
AG-3	90	600	22500	4.8	4.5	50	50
Norit-NK	67	225	5750	4.8	4.0	50	50

carbon and 35 - 38 mV for AG-3 and Norit-NK carbons. This result is in complete agreement with the conclusions of Shteinberg *et al.* [11], according to whom the electrode operates in the kinetic regime, *i.e.*, the whole inner surface of the carbon grains is equally accessible. As a consequence, the difference in activities of these three types of carbons in 1N KOH should be attributed to the difference in their true electrocatalytic activity (since the precise magnitude of the true working surface of active carbon is unknown, we refer the electrocatalytic activity to unit carbon mass, mA/g). As seen from the Table, the most active is AG-3 carbon: the ratio of activities of AG-3, Norit-NK and HS-4 in 1N KOH is approximately 3:1.5:1.

It is of interest to compare the activities of these carbons in a model electrode in 7N KOH, though in this electrolyte the electrode does not operate in a strictly kinetic regime ($i_{O_2}/i_{air} < 4.8$). The activity of all carbon types at the same E_r = 0.9 V in 7N KOH increases significantly but the ratio of the activities of AG-3 and HS-4 remains nearly the same (Table 1). At higher polarization values (E_r = 0.83 V) the difference in activity increases.

TABLE 2

Main electrode parameters of two-layer working electrodes with AG-3 active carbon

Composition of mixture	2-1	3-2	1-1	2-3
Carbon content (mg/cm^2)	20	18	15	12
i_{100} (mA/cm^2)	35	29	21	13
i'_{100} (mA/g of C)	1.75×10^3	1.6×10^3	1.4×10^3	1.88×10^3
$\frac{i'_{100} \text{ (working)}}{i'_{100} \text{ (model)}}$	0.08	0.07	0.06	0.05
ΔE_{100} (mV)	33	38	44	54
G (g of KOH/g of act. layer)	0.775	0.604	0.490	0.376
G^* (g of KOH/g of C)	1.16	1.00	0.98	0.94

TABLE 3

Main electrode parameters of two-layer working electrodes with HS-4 active carbon

Composition of mixture	2-1	3-2	1-1	2-3
Carbon content (mg/cm^2)	20	18	15	12
i_{100} (mA/cm^2)	27	28	19	11
i'_{100} (mA/g of C)	1.35×10^3	1.55×10^3	1.27×10^3	0.91×10^3
$\frac{i'_{100} \text{ (working)}}{i'_{100} \text{ (model)}}$	0.26	0.30	0.24	0.17
ΔE_{100} (mV)	46	40	50	79
G (g of KOH/g of act. layer)	0.866	0.700	0.552	0.419
G^* (g of KOH/g of C)	1.33	1.17	1.11	1.05

Apparently, in 7N KOH difficulties in oxygen mass transfer appear which have a greater effect in the case of HS-4 carbon, characterized by lower gas porosity, than in AG-3 carbon.

3.2. Working electrode

Active carbon particles which show electrocatalytic activity in oxygen reduction are like individual microelectrodes. One of the main problems is to bind these microelectrodes together with the use of a suitable binder to ensure good active layer mechanical strength without impairing its electronic and ionic conductivity, together with a sufficient mass transfer rate in the gas-filled pores. The hydrophobic component used (carbon black waterproofed with PTFE) was found to meet all these requirements. By varying the ratio of waterproofed carbon black and carbon catalyst, it is possible to vary the ratio of liquid and gas pores in the active layer over a wide range (see, *e.g.*, Fig. 5). HS-4 and AG-3 carbons, which have a significantly different ratio of lyophobic and lyophilic pores, were used as a lyophilic component in the active layer. The main electrode parameters are listed in Tables 2 and 3. It will be seen from the Tables that the optimal composition of the

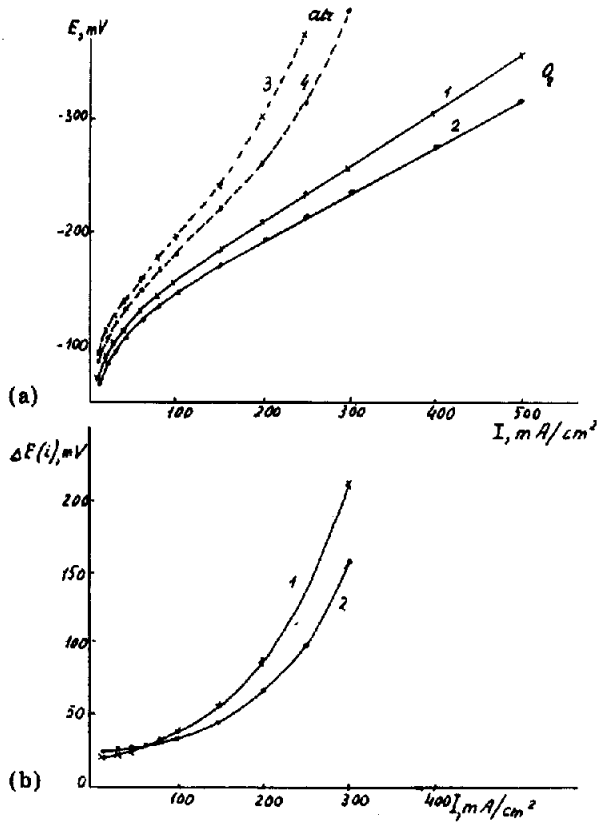

Fig. 7. (a) Polarization characteristics of oxygen (1,2) and air (3,4) working electrodes with different carbon catalysts: 1,3, HS-4 (mix 3-2); 2,4, AG-3 (mix 2-1). (b) Dependence of mass transfer hindrances in air electrodes with different carbon catalysts on current density (calculated from the curves in (a): 1, HS-4; 2, AG-3).

active layer with HS-4 carbon corresponds to a higher hydrophobic component content than with AG-3 carbon. The polarization characteristics of the electrodes of optimal composition in pure oxygen and air–oxygen are shown in Fig. 7. Notwithstanding a higher content of the hydrophobic component, in the active layer with HS-4 carbon the diffusion hindrances in air–oxygen supply appear at smaller current densities than in the layer with AG-3, which is evidenced by a faster increase in $\Delta E(i)$ in the former case (Fig. 7(b)). These results are explained by a higher active layer gas porosity with AG-3 carbon because of its intrinsic lyophobic porosity.

It is of interest to compare the specific activity per unit mass of carbon, in 7N KOH, in the working and the model floating electrodes since it allows the efficiency of the catalyst to be determined. As seen from Tables 1 - 3, at $E_{Hg/HgO} = -100$ mV ($E_r = 0.83$ V), even in the active layers of optimal composition, less than a third of the activity of the carbon catalyst is used. This means that not the whole inner surface of the carbon in the working elec-

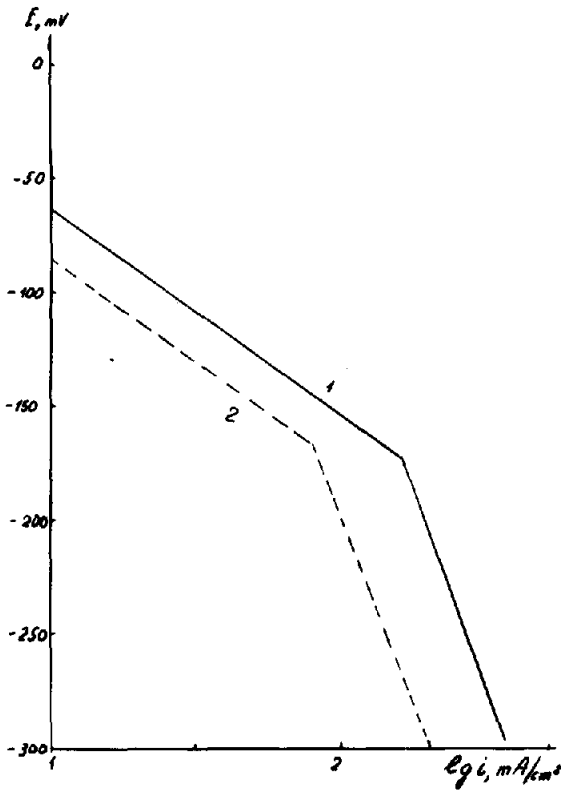

Fig. 8. Tafel plots for pure oxygen (1) and air oxygen (2) of working electrodes with a carbon catalyst.

trode is equally accessible, *i.e.* the electrode does not work in the kinetic regime and its activity is determined in high degree by mass transfer processes. This also follows from the current ratio for the working electrode i_{O_2} / $i_{air} \ll 5$ (for a model floating electrode in 7N KOH $i_{O_2}/i_{air} = 4 - 4.4$), and also from the higher slope value of the lg *i vs. E* curve than that for the model electrodes (Fig. 8). The existence of mass transfer difficulties in a working, two-layer electrode offsets to a considerable degree the difference in the initial electrocatalytic activity of HS-4 and AG-3 carbons and therefore the activity of these electrodes differs much less than in the case of model electrodes.

Figure 9 (a) shows the dependence of the electrode parameters i_{100} and ΔE_{100} and Fig. 9(b) the electrolyte content in the active layer two-layer electrodes on the catalyst–hydrophobic component ratio. These data illustrate a characteristic difference between the HS-4 and AG-3 carbons. In the first case i_{100} passes through a maximum, and in the second case rises monotonically with the increase in the amount of carbon. The parameter ΔE_{100} for HS-4 passes through a minimum, for AG-3 it diminishes monotonically. It should be noted that for both carbon catalysts the current density, i_{100}, on the electrode grows faster than the amount of carbon in the layer. Thus, for

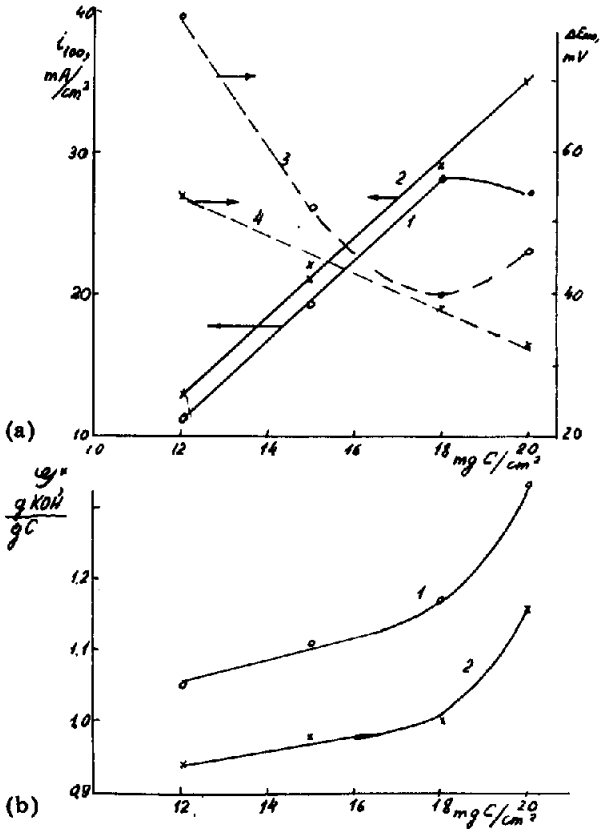

Fig. 9. (a) Dependence of i_{100} (1,2) and ΔE_{100} (3,4) on the amount of carbon catalyst for electrodes with different active carbons: 1,3, HS-4; 2,4, AG-3. (b) Dependence of electrolyte content G (g KOH/g of active layer) on the amount of carbon catalyst for electrodes with different active carbons: 1, HS-4; 2, AG-3.

example, with a 1.5 times increase in the amount of carbon (from 12 mg/cm^2 to 18 mg/cm^2) i_{100} rises by approximately 2.5 times (Fig. 9(a)). Another interesting experimental fact is that with the increase in the content of the hydrophilic component in the active layer the amount of electrolyte per unit of carbon mass, G^*, does not remain constant but increases, at first slowly, then more sharply (Fig. 9(b)). In this case the maximum value of the electrolyte content in the layer with HS-4 is higher by 0.17 cm^3 than in the layer with AG-3. An explanation of the dependences obtained follows.

At a low ratio of carbon catalyst and hydrophobic component and, accordingly, at a low liquid porosity of the active layer, a part of the carbon grains is blocked by the hydrophobic component and, as the liquid phase in the pores is unconnected with the bulk electrolyte, it does not participate in the current generation process. In other words, it can be said that the electrode works non-uniformly across its bulk due to ohmic hindrances. As the amount of carbon catalyst grows the electrolyte content in the layer in-

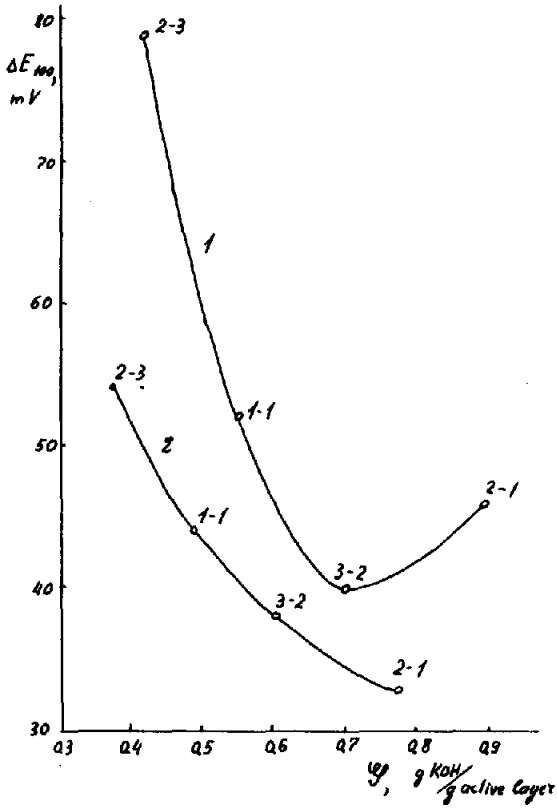

Fig. 10. Dependence of ΔE_{100} on electrolyte content G (g KOH/g of active layer) for electrodes with different carbon catalysts: 1, HS-4; 2, AG-3.

creases, not only at the expense of the liquid pores inside the active carbon grains, but also because of the filling of part of the gaps between the carbon grains, *i.e.*, the secondary structure pores. In this case previously isolated carbon grains are linked by liquid pores to form a common network and, due to this fact, the general activity increases faster than the amount of catalyst. Beginning with a certain carbon content (18 mg/cm^2 and more), the lyophilic properties of the layer are enhanced, so that electrolyte now fills a major part of the secondary structure pores, which makes oxygen transfer to active carbon grains along gas pores difficult. It leads to an increase of ΔE_{100} and a decrease of i_{100} in the electrodes with HS-4 carbon (Fig. 9(a)). The same pattern also seems to be observed in electrodes with the AG-3 catalyst, though at a smaller hydrophobic component content (less than 10 mg/cm^2). Measurements on electrodes of such composition were not performed due to their low mechanical strength. As seen from Tables 2 and 3, the efficiency of a more hydrophilic catalyst, HS-4, in a two-layer working electrode is considerably higher than that of AG-3, which confirms the existence of the ohmic hindrances in a two-layer electrode.

Figure 10 shows a strong dependence of the diffusion hindrances in the gas phase of air electrodes (ΔE_{100}) on the total electrolyte content in

the active layer. The minimum value of ΔE_{100}, just as the maximum value of i_{100} for the active layer with HS-4 catalyst, corresponds to the electrolyte content G = 0.7 g KOH/g of active layer (3-2 mix). The minimum value of ΔE_{100} for the layer with AG-3 catalyst corresponds to $G \geqslant 0.8$ g KOH/g of active layer, but this was not attained for the reasons stated earlier.

Special attention should be drawn to the fact that at a low electrolyte content the diffusion hindrances $\Delta E(i)$ in the gas phase of the air electrode are much greater, though the total gas porosity increases (Fig. 5). On the basis of the results of structural and electrochemical studies this result can be explained as follows.

As shown in Section 2, active carbon has a certain volume of lyophobic (gas) pores whose size is 1 - 2 orders larger than that of the gas pores in the hydrophobic component. As the rate of oxygen diffusion in large pores is higher than in small pores, at a sufficiently large carbon content, participation of its gas pores in the oxygen mass transfer considerably diminishes the diffusion hindrances in the air electrode. By contrast, at a low carbon content, mass transfer takes place mainly through the pores of the hydrophobic component, and $\Delta E(i)$ increases. As seen from Fig. 10, with equal electrolyte content, and even equal content of the hydrophobic component, the parameter $\Delta E(i)$ in the electrode with AG-3 carbon, having a higher volume of lyophobic pores, is less than with HS-4 carbon. This confirms the assumption of the participation of the gas pores of active carbon in the oxygen mass transfer process in the active layer. Another reason for the increase of $\Delta E(i)$ at a low electrolyte content is that due to ohmic hindrances, in this case only the carbon grains adjacent to the electrolyte side of the active layer take part in the current generation process. This is equivalent to an increase in the oxygen diffusion path to the catalyst surface, which results in greater diffusion hindrances. Similar phenomena were observed on air electrodes of the first type whose active layer consists of a mixture of catalyst and PTFE at a high content of the waterproofing agent [15].

Thus, a sharp change in the main electrode parameters with a varying ratio of the hydrophobic component and active carbon is due to a quantitative change in the volume of gas and liquid pores, on the one hand, and to qualitative changes in the mass transfer path, on the other.

References

1 A. J. Appleby, G. Crepy and G. Feuillade, in D. H. Collins (ed.), *Power Sources 6*, Academic Press, London, New York and San Francisco, 1977, p. 549.
2 O. Lindström, T. Nilsson, M. Bursell, Ch. Honell, G. Karlsson, Ch. Sylwan and B. Ahgren, in J. Thompson (ed.), *Power Sources 7*, Academic Press, London, New York and San Francisco, 1979, p. 419.
3 N. A. Urisson, G. V. Shteinberg and V. S. Bagotsky, *Elektrokhimia, 9* (1973) 1169.
4 J. Mrha, M. Musilova and J. Jindra, *Collect. Czech. Chem. Commun., 36* (1971) 638.
5 I. Iliev, S. Gamburtzev, A. Kaisheva, E. Vakanova, J. Muchovski and E. Budevski, *Commun. Dept. Chem., Bulg. Acad. Sci., 7* (1974) 223, 233.

6 I. Ilies, S. Gamburtzev, A. Kaisheva and E. Budevski, *Commun. Dept. Chem., Bulg. Acad. Sci., 8* (1975) 359.
7 I. Iliev, A. Kaisheva and G. Gamburtzev, *Commun. Dept. Chem., Bulg. Acad. Sci. 8* (1975) 367.
8 I. G. Abidor, Ya. B. Shimshelevitch and V. S. Bagotsky, *Elektrokhimia, 9* (1973) 186.
9 A. V. Dribinsky, L. N. Mokrousov, I. G. Abidor, G. V. Shteinberg, M. R. Tarasevitch and V. S. Bagotsky, *Elektrokhimia, 13* (1977) 284.
10 G. V. Shteinberg, A. V. Dribinsky, L. N. Mokrousov and I. A. Kukushkina, *28th Meeting ISE, Varna 1977, Extend. Abstr.*, v. 2, International Society of Electrochemistry, Varna-Druzhba, Bulgaria, 1977, p. 268.
11 G. V. Shteinberg, I. A. Kukushkina, V. S. Bagotsky and M. R. Tarasevitch, *Elektrokhimia, 15* (1979) 527.
12 L. N. Mokrousov, N. A. Urisson and G. V. Shteinberg, *Electrokhimia, 9* (1973) 683.
13 L. Y. Johansson, J. Mrha and R. Larsson, *Electrochim. Acta, 18* (1973) 255.
14 M. M. Dubinin, *Usp. Khim., 24* (1955) 3.
15 G. V. Shteinberg, Yu. G. Chirkov, A. P. Baranov and V. S. Bagotsky, *Elektrokhimia, 10* (1974) 322.